Long-period wurtzite-zincblende GaN polytypes as one-dimensional alloys: Impacts of stacking disorder on electronic structure and optical transitions

Anh-Luan Phan[1, a)] and Matthias Auf der Maur[1, b)]
CHOSE Centre for Hybrid Organic Solar Energy, Department of Electronic Engineering, University of Rome Tor Vergata, Via del Politecnico 1, 00133 Rome, Italy

(Dated: 26 March 2026)

The electronic structure of wurtzite-zincblende GaN polytypes is investigated by treating the stacking sequences of hexagonal and cubic bilayers as one-dimensional pseudo-binary alloys. Using an advanced atomistic empirical tight-binding scheme that is polytype-transferable, we analyze the impact of stacking disorder, namely short-range order (SRO), and internal electric polarization on the band gap, the carrier localization and the optical transitions. It is pointed out simple Ising-type models fail to capture the electronic structure of long-period polytypes due to their inability to account for quantum confinement and polarization-induced Stark effects. We also reveal that clustering of cubic or hexagonal bilayers significantly reduces the band gap, enhances carrier localization and decreases the optical transitions, an effect dramatically amplified by the internal polarization fields in the insulating regime. These results suggest that stacking disorder in GaN polytypes is not merely a defect but can be viewed as a potentially tunable degree of freedom, behaving analogously to compositional fluctuations in conventional chemical alloys.

Polytypism, the ability of a material to adopt different crystal structures based solely on the stacking sequence of atomic layers, is a hallmark of tetrahedrally bonded semiconductors like SiC[1]. In III-nitrides like GaN, while the wurtzite (WZ) phase is thermodynamically preferred, the zincblende (ZB) phase and various stacking faults are frequently observed, particularly in nanowires[2] and heteroepitaxial layers[3]. In recent years, the growth of cubic phase III-nitrides has gained increasing interest, as this would allow for example to obtain more efficient green InGaN/GaN quantum well light emitting diodes (LEDs)[4]. Traditionally, stacking variations are viewed either as discrete short-period crystallographic phases, e.g. 4H, 5T, 6H in Ramsdell notation[5] (see the visualizations in topical reviews such as Ref. 6 and Ref. 7) or as extended defects within a parent matrix[8]. However, a long-period polytype or a random stacking sequence can be conceptually mapped onto a one-dimensional (1D) pseudo-binary alloy, where the "atomic species" are the rotational-orientation character of the bilayers (hexagonal h or cubic c) and the hexagonality $\%h$ (i.e., the ratio n_h/N between number of hexagonal bilayers n_h and total number of bilayers N) plays the role of alloy concentration. Just as atomic substitution in conventional 3D chemical alloys creates disorder potentials that govern optoelectronic performance[9–11], the sequence of h and c bilayers in GaN polytypes generates a unique 1D disorder potential. A natural but open question arises: does the statistical physics of clustering and short-range order (SRO) apply to these 1D polytypic alloys in the same way it does to conventional 3D chemical alloys, and how do the strong polarization fields inherent to nitrides modify this picture?

a)anh.luan.phan@uniroma2.it
b)auf.der.maur@ing.uniroma2.it

In this Letter, we investigate the electronic structure and the optical transitions of long-period GaN polytypes, treating them as 1D alloys along the [0001]-WZ/[111]-ZB direction, labeled as z-axis, with varying degrees of stacking disorder. The number of atoms involved discourages the use of computationally heavy band-structure calculation methods like hybrid-functional density functional theory (DFT), while the Axial Next-Nearest-Neighbor Ising (ANNNI) models[12], though simple and fast, is inadequate as will be shown below. Empirical tight-binding (ETB) method[13] is a good candidate for the given problem[11]. Here we employ an advanced ETB scheme proposed in Ref. 14 and implemented in the UPTIGHT code[15], which has been shown to be transferable for various scenarios from pure bulk ones to complex ones like 3D chemical alloys or stacking polytypes[11,16]. We reuse the parameter set for GaN given in Ref. 16, noting that the slightly underestimated band gap of WZ GaN does not affect the underlying physics and our conclusions. In fact, this ETB parameter set has been shown to have high polytypic transferability, thus avoiding a conceptual contradiction of having to use distinct ETB parameter sets for GaN in different crystal phases[16] as done by the authors of Ref. 17 for GaAs. Besides, the staggered (i.e., type-II) band lineups between the two phases ZB and WZ[8,18] are automatically encoded without the need of manual adjustment.

For a given stacking configuration, we mostly followed the procedure as described in Section II of Ref. 17 to set up the ETB calculations. We also consider only two limiting regimes: the *metallic* regime, where carriers fully screen the polarization fields, and the *insulating* regime, where the unscreened polarization fields are fully active. Strain in these polytypes just gives minor corrections to atomic positions[8,19] thanks to the low lattice-mismatch as well as the high similarity in the bonding structure of the two phases. This, on the one hand, allows us to utilize a valence force field (VFF) model of Ref. 20 and choosing

TABLE I. Material parameters of GaN in WZ and ZB phases. The lattice parameters (a, c, u) of ZB are derived from the ZB lattice constant 0.4531 nm[24].

Parameter	WZ		ZB
a (nm)	0.3189[25]		0.3204
c (nm)	0.5185[25]		0.5232
u	0.3768[20]		0.3750
α (N/m)		88.35[20]	
β (N/m)		20.92[20]	
P_z^f (C/m^2)	1.312[23]		1.347[23]
e_{14} (C/m^2)			0.6[26]
e_{31} (C/m^2)	−0.551[23]		
e_{33} (C/m^2)	1.020[23]		
ϵ (ϵ_0)	8.9[27]		9.7[27]

the same VFF parameters α and β in both phases for simplicity; on the other hand, it implies that the non-linear piezoelectric response can be safely ignored[21]. There are, however, two considerable differences in our simulation workflow compared to Ref. 17. Firstly, we generally do not assume extended domains of WZ or ZB phases, instead each Ga-N bilayer is uniquely and unambiguously recognized as either hexagonal (h) or cubic (c) [see Fig. 5 of Ref. 6 for an illustration; a simple rule: if two adjacent bilayers of a given bilayer are the same (e.g., both are A) then that given bilayer is hexagonal, otherwise it is cubic]. Secondly, we used the correct implementation[22,23] to calculate the polarization differences at the hypothetical interfaces between adjacent bilayers, which were set at the z-coordinates of the Ga atoms for simplicity. Namely, the z-component of the net polarization in each bilayer reads (assuming linear piezoelectricity):

$$P_z^{\text{net}} = P_z^f + 2(e_{31} - P_z^f)\varepsilon_\perp + e_{33}\varepsilon_\parallel. \quad (1)$$

where P_z^f is the z-component of the formal polarization, $\varepsilon_{\perp,\parallel}$ are the in-plane/out-of-plane strains, while $e_{31,33}$ are the *proper* linear piezoelectric coefficients (i.e., the ones corresponding to experimental measurements). For cubic bilayers (ZB), we can derive the effective proper $e_{31,33}$ from the proper e_{14} coefficient via:

$$e_{31} = -e_{14}/\sqrt{3}, \quad e_{33} = 2e_{14}/\sqrt{3}. \quad (2)$$

Although the above way of polarization calculation is conceptually different from the common (but *incorrect*) practice in the field, we verified that the numerical differences are modest in our case. The bulk material parameters needed for the simulations are shown in Table I, including: the lattice parameters (a, c, u), the VFF parameters (α, β), z-component of the formal polarization (P_z^f), the proper piezoelectric coefficients (e_{14}, e_{31}, e_{33}) and the relative dielectric constants (ϵ).

We first address the limitation of Ising-type models for predicting polytypes' band-gaps by comparing our ETB with the ANNNI "Model 4" in Ref. 7 using the band-gaps

TABLE II. Parameters of the ANNNI "Model 4" in Ref. 7 fitted to our ETB gaps. All values are in eV.

Regime	$\mathbf{J_0}$	$\mathbf{J_1}$	$\mathbf{J_2}$	$\mathbf{J_3}$	$\mathbf{K}$
Metallic	3.2227	0.0249	0.0010	0.0007	0.0009
Insulating	3.2225	0.0250	0.0011	0.0006	0.0006

of 497 short-period GaN polytypes with $N \leq 15$ bilayers (see List S1 in Supplementary Information of Ref. 7). For a fair comparison, we used our ETB gaps of small polytypes 2H, 4H, 3C, 5T and 6T in each regime to refit the parameters of the ANNNI model, as given in Table II. The ANNNI parameters in two regimes are almost the same because for the small polytypes used for fitting, the polarization effect has very little impact on the band-gap values. Figure 1 reveals the limitations of the ANNNI model for band-gap prediction compared to the atomistic ETB method. In the metallic regime, the ETB gaps follow a roughly linear trend with hexagonality, whereas in the insulating regime, a large number of ETB gaps lying drastically lower than the linear interpolation. The ANNNI model, on the other hand, predicts almost linear trend in both regimes with the gaps slightly *higher* than the linear interpolation and fails to capture the strong gap reduction observed in insulating regime as the ETB method did. Note that a similar linear trend was also demonstrated in Figure 4 of Ref. 7 although the authors fitted their ANNNI parameters to the hybrid-functional-DFT gaps, indicating that the wrong prediction is due to the inadequate physics of the ANNNI model and not from the choice of the fitting targets. In fact, the parameters of the ANNNI model were derived merely from the band-gap values of some short-period polytypes (up to 6 bilayers), thus its predictions for short-period polytypes may match fairly well to the corresponding values of the genuine band-structure methods like DFT or ETB, as verified in Ref. 7 for polytypes of $7-8$ bilayers. However, for longer-period ones, the discrepancies in band-gap predictions become more obvious because the Ising-type models are blind to the underlying mechanism of how the electrons and holes are confined in the structures — a point that we will try to clarify in the remaining part of this Letter.

To elucidate such mechanism, we analyze two distinct polytypes with identical period ($N = 15$) and hexagonality ($\%h = 40\%$), indexed as "310" and "492" (see List S1 in Ref. 7). In the metallic regime, their gaps differ by only 7 meV (3.211 eV vs. 3.218 eV, respectively). However, in the insulating regime, this difference increases to ~ 50 meV (3.169 eV vs. 3.218 eV, respectively). In Figure 2 we plot their band-edge profiles along the stacking direction. One can see that polytype "310" is a highly clustered configuration (stacking sequence *chhhhhhccccccc*), creating extended domains of WZ and ZB phases. In the metallic regime, these form flat quantum wells (QWs) for holes (in the WZ domains) and electrons (in the ZB domains). In

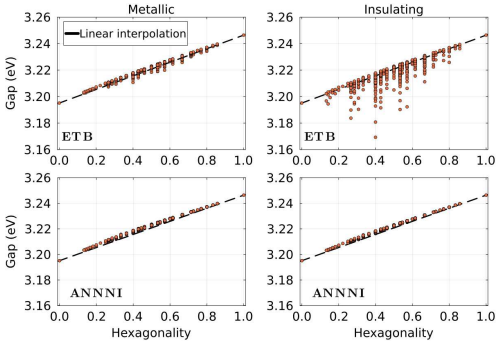

FIG. 1. Band-gaps of 497 GaN polytypes with period up to $N = 15$ bilayers calculated by ETB (top) and ANNNI (bottom) in the metallic (left) and insulating (right) regimes. The dashed line represents the linear interpolation between the gaps of ZB phase (3C, $\%h = 0\%$) and WZ phase (2H, $\%h = 100\%$).

the insulating regime, the polarization discontinuities at the hexagonal-cubic interfaces introduce strong electric fields with opposite signs in the two layers. This leads to a reduction in the electronic band gap — the well-known quantum-confined Stark effect (QCSE)[28]. Conversely, polytype "492" (stacking sequence *chchcchchcchchc*) has a distributed stacking configuration. The potential fluctuations are rapid and shallow, preventing the formation of deep confined states. Consequently, the polarization effect is negligible for such alternating structures, and the insulating gap remains close to the metallic value. This result underscores that the specific bilayer *arrangement* (microstructure) of the polytype — not just the global hexagonality — determines its electronic structure, fundamentally behaving as 1D disordered alloys.

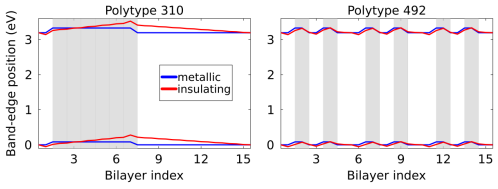

FIG. 2. Band-edge profiles for two 15-bilayer polytypes, "310" (left) and "492" (right), in both metallic (blue) and insulating (red) regimes. Both polytypes have identical hexagonality ($\%h = 40\%$) but with distinct stacking sequences. Polytype "310" exhibits strong clustering, creating deep QWs in insulating regime, while polytype "492" is more distributed. The background shading indicates the bilayer character (grey for hexagonal, white for cubic).

To investigate further such alloy-like behavior, we consider long-period GaN polytypes with $N = 30,\ 50,\ 100$ in full range of hexagonality $\%h$. For each given pair $\{N, \%h\}$, we performed ETB calculations on an ensemble of 100 different stacking configurations in which bilayers of each character are distributed in a completely random manner. Figure 3 shows the variations of the band-gap versus hexagonality for different number of bilayers, along with the corresponding degrees of statistical scattering. Clearly, the band-gap bowing increases with N especially in insulating regime, and so does the statistical scattering. This is reasonable because in long-period polytypes, it is more likely to form extended domains of WZ or ZB phases even in a perfectly random distribution.

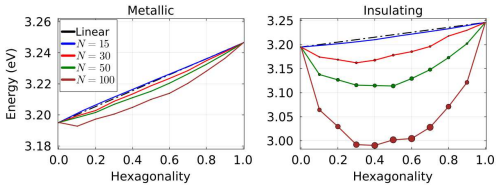

FIG. 3. Band-gap variations (mean values) versus hexagonality for polytypes with different periods in two regimes: metallic (left) and insulating (right). The marker sizes are proportional to the standard deviations.

Similar to normal alloys[29], deviations from a perfectly random distribution like SRO can have important effects on the electronic structure. We characterized the SRO via the Cowley parameters[30] $\alpha \equiv \alpha_1$ as in Ref. 10, where $\alpha = 0$ represents a perfectly random distribution as above, while $\alpha > 0$ promotes clustering tendency (i.e., association of like-character bilayers) and $\alpha < 0$ corresponds to anti-clustering tendency. Stacking ensembles for each desired value of α were generated using the reverse Monte Carlo algorithm[31,32]. The influence of SRO is systematically explored in Figure 4, which shows the band-gap variations for polytypes of $N = 100$ with different values of Cowley parameter α. In the metallic regime, the dependence on α is present but weak. In the insulating regime, however, the effect is much more profound. Polytypes with clustering tendency ($\alpha > 0$) exhibit significantly smaller band gaps compared to random ($\alpha = 0$) or anti-clustered ($\alpha < 0$) configurations. A clustering sequence maximizes the width of the WZ and ZB domains. As predicted by the QW physics discussed above, wider wells lead to lower confinement energies and stronger QCSE redshifts. Conversely, anti-clustering tendency implies alternating h and c bilayers (e.g., *hchchc*), which effectively behaves as short-period polytypes with higher band-gaps. This statistical analysis confirms that "alloy disorder" in the stacking sequence — specifically the formation of clusters — is a potent mechanism for band-gap narrowing in GaN polytypes. In fact, previous experimental works[33,34] measured the emission energies from ensembles of WZ GaN nanowires with ZB stacking faults and found broad distributions — an indication of "alloy disorder". Notably, many peaks lie far below the

bulk ZB GaN band gap, which is consistent with our ETB results showing gap reduction in polytypes with extended ZB domains.

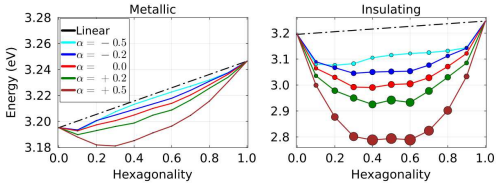

FIG. 4. Band-gap variations versus hexagonality for polytypes of $N = 100$ bilayers in two regimes: metallic (left) and insulating (right), with different Cowley parameter α.

Furthermore, we used the inverse participation ratio (IPR) as shown in Figure 5 to quantify the degrees of localization of the conduction-band-edge (CBE) and valence-band-edge (VBE) states. In WZ and ZB polytypes, the wavefunction density is of course delocalized uniformly among bilayers, thus IPR $= 1/N = 0.01$ when scaled to $N = 100$. In case IPR $= 1$, we have a completely localized state; otherwise with $0.01 <$ IPR < 1 the state is partially localized. From Figure 5 one can see that clustering tendency consistently enhances the localization of both band-edge states, while the anti-clustering tendency does the opposite. As expected, the polarization effect in insulating regime amplifies the carrier confinement due to deepened QWs.

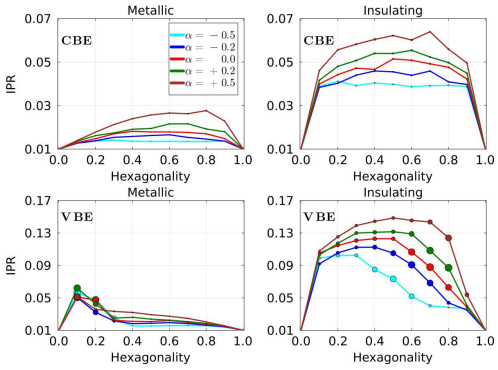

FIG. 5. Variations of the IPR of the CBE (top) and VBE (bottom) states versus hexagonality for polytypes of $N = 100$ bilayers in metallic (left) and insulating (right), with different Cowley parameter α.

Figure 6 visualizes the probability distribution of the band-edge states for a representative clustered polytype ($N = 100$, $\%h = 30\%$, $\alpha = 0.5$) and the corresponding band-edge profiles. In the metallic regime, the electron (CBE) and hole (VBE) are relatively delocalized over the

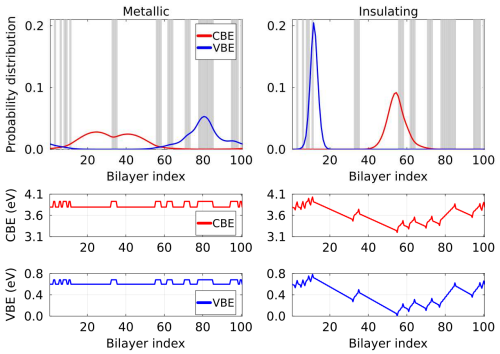

FIG. 6. *Top:* Probability distribution ($|\psi|^2$) of the CBE (red) and VBE (blue) states for a representative polytype of $N = 100$, $\%h = 30\%$, $\alpha = 0.5$ in two regimes: metallic (left) and insulating (right). The background shading indicates the bilayer character (grey for hexagonal, white for cubic). *Middle and bottom:* The corresponding band-edge profiles.

polytype. Because the QWs in this regimes are flat, the states tend to be localized in the middle of the QWs. In the insulating regime, the polarization fields break the symmetry. The QWs are not only deepened, but also have triangular shapes with steeper slope on the hexagonal side. As a result, the hole and electron wavefunctions become strongly localized at one of the hexagonal-cubic interfaces, slightly leaning on the cubic side. The electron wavefunction experiences this strong confinement less severely due to its lighter effective mass. As already known from the QCSE, the spatial separation between hole and electron wavefunctions is increased while the overlap between them is significantly diminished. This aligns with an experimental observation[34] on the increase of the initial decay time of time-resolved photoluminescence with increased ZB-inclusion thickness. However, for structures whose the built-in electric fields are weak or screened, the attractive Coulomb interaction between hole and electron can partly overcome the wavefunction separation, causing slightly enhanced overlap with increasing ZB-inclusion thickness before the overlap eventually follows the decreasing trend[35].

From the reduced electron-hole overlap, one can expect a significant drop in the optical strength of the ground-state transition. This is indeed confirmed in Figure 7, which shows the squared module of the ground-state optical matrix element, $|\mathbf{P}|^2$. Together with Figure 5, one can see strong correlations between the degree of SRO with respect to the carrier localization and the optical transitions. Clustering causes the localization enhancement, decreasing electron-hole wavefunction overlap and consequently the drop in optical strength. The role of the internal electric polarization is amplifying this effect, increasing the degree of confinement and making the optical strength drop even more.

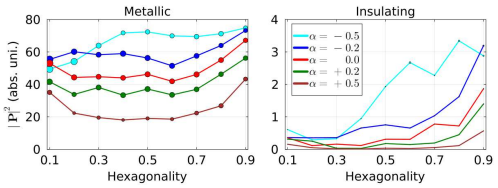

FIG. 7. Squared module of the ground-state optical matrix element $|\mathbf{P}|^2$ versus hexagonality for polytypes of $N = 100$ bilayers in two regimes: metallic (left) and insulating (right), with different Cowley parameter α.

In conclusion, using an advanced ETB scheme we have established that long-period GaN polytypes behave essentially as 1D pseudo-binary alloys where stacking disorder dictates the optoelectronic properties. We demonstrated that the band gap is not merely a function of hexagonality but is critically sensitive to the SRO. Clustering of like-character bilayers significantly reduces the band gap, induces strong carrier localization and decreases the optical transitions, an effect magnified by the internal polarization fields. Standard Ising-type ANNNI models fail to capture these effects, while the hybrid-functional DFT is too expensive to be utilized in this context. Although no direct experimental benchmark currently exists, consistency of the physical picture in our work with available experiments[33,34] can be found.

Our results suggest that controlling the statistics of stacking faults — effectively engineering the Cowley SRO parameter α — offers a pathway to tune the emission wavelength, carrier localization and optical emission strength in group-III nitride metamorphic heterostructures, beyond conventional chemical alloying. On the other hand, our theoretical work pointed out that alternating stacking configurations (i.e., $\alpha < 0$) help in reducing the QCSE, thus should exhibit larger band gaps and better optical emission intensity. A recent experimental study[36] demonstrated the possibility of growing such GaN structures via appropriate growth conditions, suggesting the potential of misfit-dislocation-free homo-epitaxial UV-A light emitting devices. As a final note, our calculation framework here is not specific for GaN, but can be applied similarly to investigate the wurtzite-zincblende stacking polytypes of other tetrahedrally bonded materials.

ACKNOWLEDGMENTS

This work has been supported by European Union's Horizon 2020 research and innovation programme under the Marie Skłodowska-Curie grant agreement n° 956548, project Quantimony. Matthias Auf der Maur acknowledges support by the European UnionNextGenerationEU under the Italian National Center 1 on HPCSpoke 6: "Multiscale Modelling and Engineering Applications" MUR CUP: E83C22003230001.

AUTHOR DECLARATIONS

Conflict of Interest

The authors have no conflicts to disclose.

Author contributions

Anh-Luan Phan: Conceptualization (lead); formal analysis (lead); investigation (lead); methodology (lead); software (lead); visualization (lead); writing – original draft (lead); writing – review and editing (lead). **Matthias Auf der Maur:** Conceptualization (supporting); formal analysis (supporting); funding acquisition (lead); methodology (supporting); resources (lead); supervision (lead); validation (lead); writing – review and editing (supporting).

DATA AVAILABILITY

The data that support the findings of this study are available within the article.

[1] P. Krishna and A. R. Verma, physica status solidi (b) **17**, 437 (1966).
[2] W. Rieger, R. Dimitrov, D. Brunner, E. Rohrer, O. Ambacher, and M. Stutzmann, Physical Review B **54**, 17596 (1996).
[3] M. Albrecht, S. Christiansen, G. Salviati, C. Zanotti-Fregonara, Y. T. Rebane, Y. G. Shreter, M. Mayer, A. Pelzmann, M. Kamp, K. J. Ebeling, M. D. Bremser, R. F. Davis, and H. P. Strunk, MRS Proceedings **468**, 293 (1997).
[4] J. Lee and C. Bayram, Applied Physics Letters **124**, 011101 (2024).
[5] L. S. Ramsdell, American Mineralogist **32**, 64 (1947).
[6] F. Bechstedt and A. Belabbes, Journal of Physics: Condensed Matter **25**, 273201 (2013).
[7] R. Ramakrishnan and S. Jain, The Journal of Chemical Physics **159**, 124702 (2023).
[8] C. Stampfl and C. G. Van De Walle, Physical Review B **57**, R15052 (1998).
[9] K. A. Mäder and A. Zunger, Applied Physics Letters **64**, 2882 (1994).
[10] L. Bellaiche and A. Zunger, Physical Review B **57**, 4425 (1998).
[11] A.-L. Phan, A. Pecchia, A. Di Vito, and M. Auf der Maur, Physica Scripta **99**, 075903 (2024).
[12] J. Von Boehm and P. Bak, Physical Review Letters **42**, 122 (1979).
[13] J. C. Slater and G. F. Koster, Physical Review **94**, 1498 (1954).
[14] Y. Tan, M. Povolotskyi, T. Kubis, T. B. Boykin, and G. Klimeck, Physical Review B **94**, 045311 (2016).
[15] "Uptight," https://github.com/tiberlab/uptight (2025).
[16] A.-L. Phan, D. Soccodato, A. Pecchia, A. Di Vito, and M. Auf der Maur, Physical Review B **112**, 165202 (2025).
[17] J. Sink and C. Pryor, Physical Review B **108**, 075104 (2023).
[18] X. H. Lu, P. Y. Yu, L. X. Zheng, S. J. Xu, M. H. Xie, and S. Y. Tong, Applied Physics Letters **82**, 1033 (2003).
[19] A. Benbedra, S. Meskine, A. Boukortt, R. Hayn, M. Texier, O. Thomas, and T. W. Cornelius, Computational Condensed Matter **43**, e01033 (2025).

[20]D. Camacho and Y. Niquet, Physica E: Low-dimensional Systems and Nanostructures **42**, 1361 (2010).
[21]P.-Y. Prodhomme, A. Beya-Wakata, and G. Bester, Physical Review B **88**, 121304 (2013).
[22]D. Vanderbilt, Journal of Physics and Chemistry of Solids **61**, 147 (2000).
[23]C. E. Dreyer, A. Janotti, C. G. Van De Walle, and D. Vanderbilt, Physical Review X **6**, 021038 (2016).
[24]O. Madelung, *Semiconductors: Data Handbook*, 3rd ed. (Springer Berlin Heidelberg, Berlin, Heidelberg, 2004).
[25]I. Vurgaftman and J. R. Meyer, Journal of Applied Physics **94**, 3675 (2003).
[26]A. D. Bykhovski, V. V. Kaminski, M. S. Shur, Q. C. Chen, and M. A. Khan, Applied Physics Letters **68**, 818 (1996).
[27]M. E. Levinshteĭn, S. L. Rumyantsev, and M. Shur, eds., *Properties of Advanced Semiconductor Materials: GaN, AlN, InN, BN, SiC, SiGe* (Wiley, New York, 2001).
[28]D. A. B. Miller, D. S. Chemla, T. C. Damen, A. C. Gossard, W. Wiegmann, T. H. Wood, and C. A. Burrus, Physical Review Letters **53**, 2173 (1984).
[29]A. Di Vito, A. Pecchia, A. Di Carlo, and M. Auf der Maur, Physical Review Applied **12**, 014055 (2019).
[30]J. M. Cowley, Journal of Applied Physics **21**, 24 (1950).
[31]R. L. McGreevy and L. Pusztai, Molecular Simulation **1**, 359 (1988).
[32]D. A. Keen, M. G. Tucker, and M. T. Dove, Journal of Physics: Condensed Matter **17**, S15 (2005).
[33]G. Jacopin, L. Rigutti, L. Largeau, F. Fortuna, F. Furtmayr, F. H. Julien, M. Eickhoff, and M. Tchernycheva, Journal of Applied Physics **110**, 064313 (2011).
[34]J. Lähnemann, U. Jahn, O. Brandt, T. Flissikowski, P. Dogan, and H. T. Grahn, Journal of Physics D: Applied Physics **47**, 423001 (2014).
[35]P. Corfdir and P. Lefebvre, Journal of Applied Physics **112**, 053512 (2012).
[36]C. Guérin, F. Jourdan, B. Moreau, B. Gayral, J.-L. Rouvière, G. Jacopin, and B. Daudin, Journal of Applied Physics **138**, 035304 (2025).